Dalton Transactions

ROYAL SOCIETY OF CHEMISTRY

PAPER

View Article Online
View Journal | View Issue

Cite this: *Dalton Trans.*, 2025, **54**, 2599

Triazolyl-phosphole and triazolyl-azaphosphole: synthesis, transition metal complexes and catalytic studies†‡

Latchupatula Radhakrishna, Basvaraj S. Kote, Rani Gourkhede, Ankit Pandey, Bhupinder Kaur and Maravanji S. Balakrishna *

Received 16th November 2024,
Accepted 12th December 2024

DOI: 10.1039/d4dt03213f

rsc.li/dalton

Phosphole and azaphosphole derivatives with triazole functionalities, [C_6H_5{1,2,3-$N_3CC_6H_4C(PPh)$}] (**L1**) and [C_6H_4{1,2,3-$N_3C(Ph)C(PPh)$}] (**L2**) were synthesized by reacting [(C_6H_5)(1,2,3-N_3C = CH-*o*-Br-C_6H_4)] and [(*o*-Br-C_6H_4)(1,2,3-N_3C = CHC_6H_5)] with ^{n}BuLi followed by the addition of dichlorophenylphosphine. The reactions of **L1** and **L2** with an excess of 30% H_2O_2 afforded phosphole oxides [C_6H_5{1,2,3-$N_3CC_6H_4C(P(O)Ph)$}] (**L1$_O$**) and [C_6H_4{1,2,3-$N_3C(Ph)C(P(O)Ph)$}] (**L2$_O$**) as white crystalline solids. Stoichiometric reactions of **L1** and **L2** with [Ru(η^6-*p*-cymene)Cl_2]$_2$ in CH_2Cl_2 yielded [$RuCl_2$(η^6-*p*-cymene)(**L1**-κ^1-*P*)] (**1**) and [$RuCl_2$(η^6-*p*-cymene)(**L2**-κ^1-*P*)] (**2**), respectively. Similar reactions of **L1** and **L2** with [Pd(COD)Cl_2] and [Pd(η^3-C_3H_5)Cl]$_2$ produced the corresponding complexes, *trans*-[$PdCl_2$(**L1**-κ^1-*P*)$_2$] (**3**), *trans*-[$PdCl_2$(**L2**-κ^1-*P*)$_2$] (**4**), [Pd(η^3-C_3H_5)Cl(**L1**-κ^1-*P*)] (**5**), and [Pd(η^3-C_3H_5)Cl(**L2**-κ^1-*P*)] (**6**). Treatment of **L1** with [AuCl(SMe_2)] in dichloromethane afforded [AuCl(**L1**-κ^1-*P*)] (**7**). Ruthenium complex **1** showed moderate to good catalytic activity towards benzylic C–H oxidation, and the proposed mechanism for the catalysis was supported by spectroscopic data.

Introduction

Phospholes have emerged as a significant area of interest within heterocyclic π-conjugated systems due to their versatile applications in organic electronics,[1] catalysis,[2] and related fields.[3] The phosphole ring with a highly reactive phosphorus atom, exhibits unique properties including low aromaticity and σ–π hyperconjugation, making it a valuable building block for advanced molecular designs.[4] These compounds can be synthesized through various strategies tailored to achieve specific structural and functional attributes. A widely employed method is the [4 + 1] cycloaddition of 1,3-diynes with primary phosphines, enabling efficient construction of the phosphole framework.[5] Additionally, dehydrohalogenation and dehalogenation reactions using lithium reagents facilitate ring closure *via* halide elimination.[6] Metal-catalyzed techniques further provide efficient and versatile pathways for the synthesis of diverse phosphole derivatives.[7]

The first examples of phosphole oxides featuring 1,2,3-triazoles at the α-position were reported by Matano and co-workers.[8] These compounds were synthesized *via* the Cu(I)-catalyzed azide–alkyne cycloaddition (CuAAC) reaction between ethynylphosphole *P*-oxides and aryl azides, achieving moderate to high yields (Chart 1, **I–III**). Additionally, Baumgartner and co-workers described the synthesis of *P*-triazole dithienophospholes, wherein the triazole ring is directly coordinated to the phosphorus atom (Chart 1, **IV**).[9] To the best of our knowledge, phospholes fused with triazole rings and also azaphospholes are not known in the literature. Compounds incorporating fused triazole, phenyl, and phosphole units represent a distinctive combination of structural components. The triazole[10] offers a heterocyclic structure that supports strong coordination interactions, while the phenyl group enhances aromatic stability. The phosphole moiety, characterized by its electron-rich phosphorus center, provides additional coordination sites, facilitating interactions with metals or other electrophilic species.

Complexes with phosphole ligands have demonstrated diverse applications in catalysis, including hydrogenation,[11] carbonylation,[12] and coupling reactions.[13] C–H bond oxidation is one of the most fundamental chemical processes in synthesizing natural products, agrochemicals, pharmaceuticals and

Phosphorus Laboratory, Department of Chemistry, Indian Institute of Technology Bombay, Powai, Mumbai 400076, India. E-mail: krishna@chem.iitb.ac.in, msb_krishna@iitb.ac.in

† Dedicated to Prof. Vadapalli Chandrasekhar in celebration of his 65th birthday.

‡ Electronic supplementary information (ESI) available: Tables of selected structural data and selected spectroscopic data. CCDC 2403173, 1832215 and 2403174 For ESI and crystallographic data in CIF or other electronic format see DOI: https://doi.org/10.1039/d4dt03213f

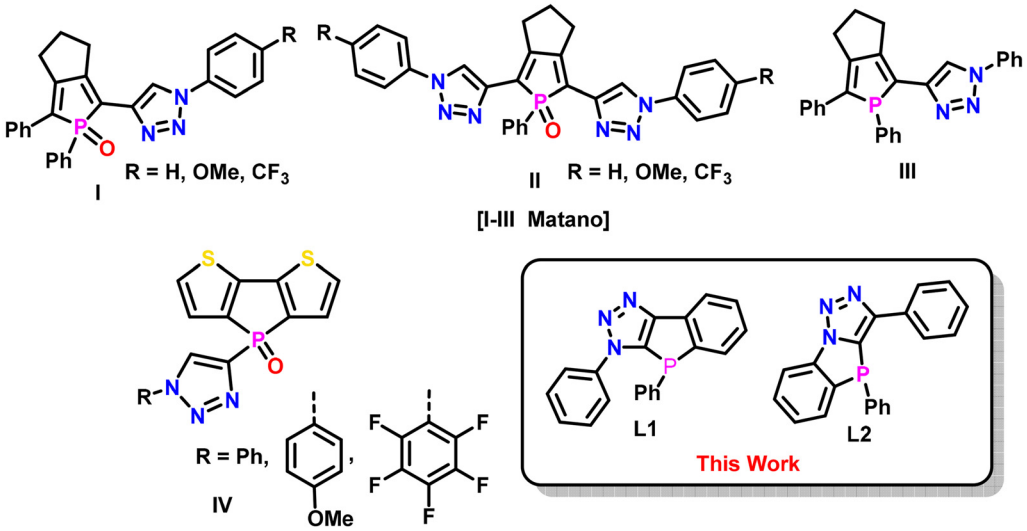

Chart 1 Phosphole appended ligands.

several other important transformations.[14] Direct conversion of a methylene group into a carbonyl group is a desirable synthetic objective for which complexes containing chromium,[15] manganese,[16] iron,[17] ruthenium,[17,18] cobalt,[19] rhodium[20] and gold[21] act as catalysts in the presence of oxidants such as OsO_4, ^tBuOOH, $(NH_4)_2Ce(NO_3)_6$, $NaIO_4$. However, still enormous potential is there to find better catalysts to tolerate a broad range of substrates with different functional groups.

In this paper we describe the synthesis and transition metal chemistry of phosphole and azaphosphole ligands [C_6H_5{1,2,3-$N_3CC_6H_4C(PPh)$}] (**L1**) and [C_6H_4{1,2,3-$N_3C(Ph)C(PPh)$}] (**L2**) based on a 1,2,3-triazole core. The ruthenium(II) complex [$RuCl_2(\eta^6$-*p*-cymene){C_6H_5(1,2,3-$N_3CC_6H_4C(PPh)$)-κ^1-*P*}] (**1**) catalysed the benzylic C–H oxidation reaction under aerobic conditions efficiently.

Results and discussion

Synthesis of [C_6H_5{1,2,3-$N_3CC_6H_4C(PPh)$}] (L1), [C_6H_4{1,2,3-$N_3C(Ph)C(PPh)$}] (L2), [C_6H_5{1,2,3-$N_3CC_6H_4C(P(O)Ph)$}] ($L1_O$), and [C_6H_4{1,2,3-$N_3C(Ph)C(P(O)Ph)$}] ($L2_O$)

Bromo-triazole derivatives (**A** and **B**) were synthesized using the modified procedure recently published by our group.[22] The reactions of phenyl azide or 2-bromophenyl azide with 2-bromophenylacetylene or phenylacetylene in the presence of copper sulfate and sodium ascorbate afforded 4-(2-bromophenyl)-1-phenyl-1*H*-1,2,3-triazole **A** and 1-(2-bromophenyl)-4-phenyl-1*H*-1,2,3-triazole **B**, respectively, as white crystalline solids. The reactions of triazole derivatives **A** and **B** with ^nBuLi followed by the addition of $PhPCl_2$ afforded phosphole derivatives [C_6H_5{1,2,3-$N_3CC_6H_4C(PPh)$}] (**L1**) and [C_6H_4{1,2,3-$N_3C(Ph)C(PPh)$}] (**L2**), respectively, as air-stable white crystalline solids, soluble in most of the organic solvents (Scheme 1). The reactions of **L1** and **L2** with an excess of H_2O_2 afforded oxide derivatives [C_6H_5{1,2,3-$N_3CC_6H_4C(P(O)Ph)$}] ($L1_O$) and [C_6H_4{1,2,3-$N_3C(Ph)C(P(O)Ph)$}] ($L2_O$), respectively (Scheme 1). The $^{31}P\{^1H\}$ NMR spectra of **L1** and **L2** showed single resonances at −39.5 and −32.9 ppm (Fig. S3 and S7‡), whereas the same due to oxides $L1_O$ and $L2_O$ appeared at 11.5 and 14.1 ppm (Fig. S12 and S16‡). The ^1H NMR spectra confirmed the absence of triazolic C–H proton (which appear at 8.42 and 8.52 ppm). HRMS spectra of compounds **L1** and **L2** showed molecular ion peaks at 328.0997 and 328.0991, respectively, corresponding to $[M + H]^+$ ions, whereas those of $L1_O$ and $L2_O$ observed at 344.0941 corresponding to $[M + H]^+$ ion (Fig. S6, S10, S14 and S18‡).

Molecular structures of [C_6H_5{1,2,3-$N_3CC_6H_4C(PPh)$}] (L1) and [C_6H_4{1,2,3-$N_3C(Ph)C(PPh)$}] (L2)

The perspective views of the molecular structures of **L1** and **L2** are shown in Fig. 1. The compound **L1** crystallized in the triclinic system with the $P\bar{1}$ space group, whereas the compound **L2** crystallized in the monoclinic system with the $P2_1/c$ space group. The pyramidal geometries around the P atoms (∠C1–P1–C15 = 102.77(7)°, ∠C1–P1–C8 = 87.13(7)°, ∠C15–P1–C8 = 100.64(7)° in **L1** and ∠C15–P1–C4 = 100.7(3)°, ∠C19–P1–C15 = 102.6(3)°, ∠C19–P1–C4 = 87.4(3)°) in **L2** are slightly distorted. The P1–C1 bond distances in **L1** (1.8051(16) Å) and **L2** (1.942 (13) Å) are similar to that found in [C_6H_5{1,2,3-N_3C(*o*-$Ph_2P(C_6H_4)$)$C(PPh_2)$}].

Synthesis of Ru(II) complexes [$RuCl_2(\eta^6$-*p*-cymene)(L1-κ^1-*P*)] (1) and [$RuCl_2(\eta^6$-*p*-cymene)(L2-κ^1-*P*)] (2)

Reactions of **L1** and **L2** with $[Ru(\eta^6$-*p*-cymene$)Cl_2]_2$ in 2 : 1 ratios in dichloromethane resulted in mononuclear complexes [$RuCl_2(\eta^6$-*p*-cymene)(**L1**-κ^1-*P*)] (**1**) and [$RuCl_2(\eta^6$-*p*-cymene)(**L2**-κ^1-*P*)] (**2**), in good yield as shown in Scheme 2. The $^{31}P\{^1H\}$ NMR spectra of complexes **1** and **2** showed single resonances at −0.1 and −3.9 ppm, respectively (Fig. S20 and S25‡). The aliphatic

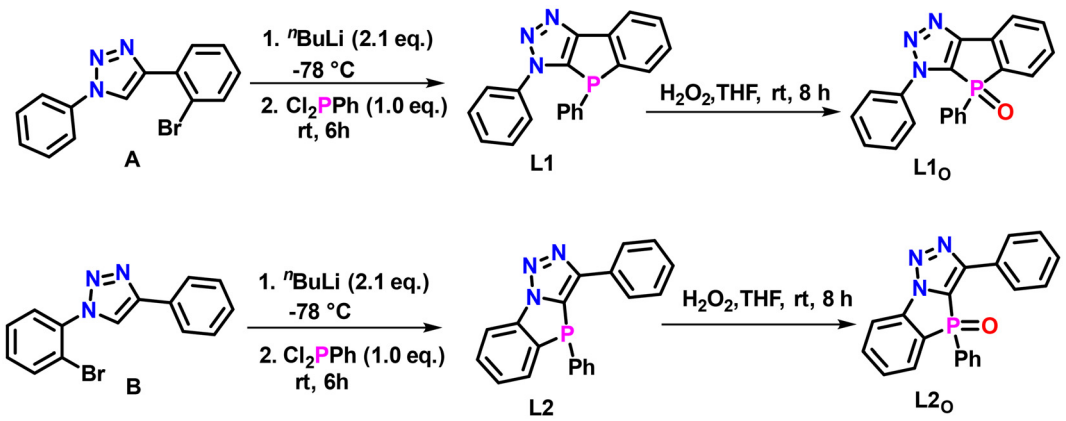

Scheme 1 Synthesis of phosphole, azaphosphole and their oxides.

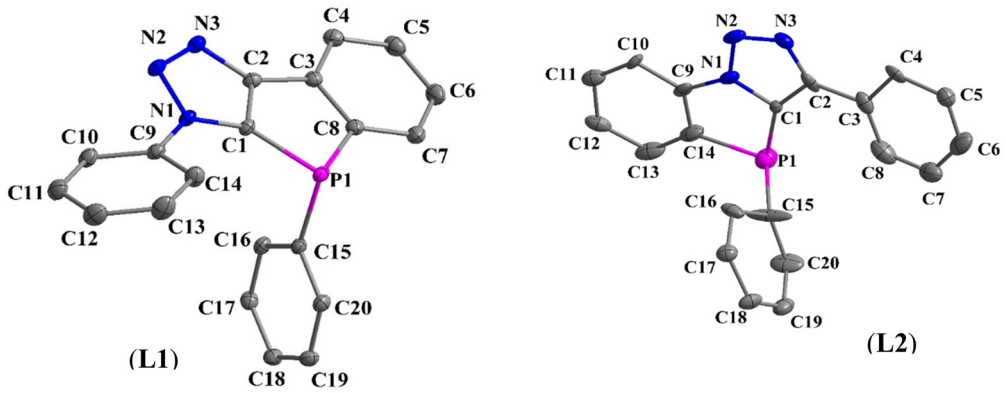

Fig. 1 Molecular structures of $[C_6H_5\{1,2,3\text{-}N_3CC_6H_4C(PPh)\}]$ (**L1**) and $[C_6H_4\{1,2,3\text{-}N_3C(Ph)C(PPh)\}]$ (**L2**) with 30% thermal ellipsoids (H atoms have been omitted for clarity). Selected bond lengths (Å) and bond angles (°): compound **L1**: C1–P1 1.8057(16), C8–P1 1.8454(18), C15–P1 1.8325(17), C1–P1–C15 = 102.77(7) °, C1–P1–C8 = 87.13(7) °, C15–P1–C8 = 100.64(7) °; compound **L2**: C1–P1 1.942(13), C15–P1 1.983(7), C14–P1 1.942(9), C15–P1–C4 = 100.7(3)°, C19–P1–C15 = 102.6(3)°, C19–P1–C4 = 87.4(3)°.

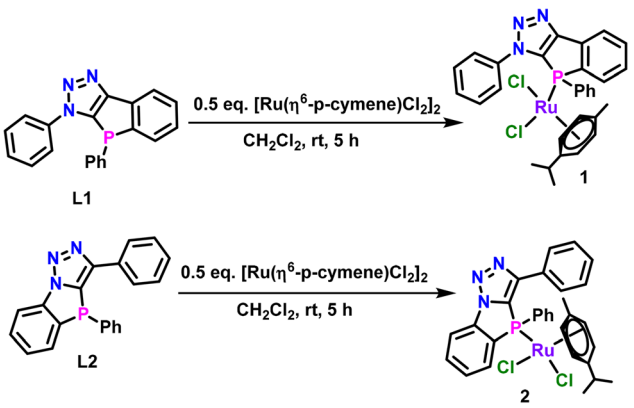

Scheme 2 Synthesis of Ru^{II} complexes **1** and **2**.

protons of the *p*-cymene group revealed a septet at 2.27 ppm, two doublets at 0.91 and 0.83 ppm with a $^3J_{HH}$ coupling of 6.9 Hz for the isopropyl group, and a singlet at 1.27 ppm for the methyl group. HRMS spectra of compounds **1** and **2** showed a molecular ion peak at 571.9854 corresponding to $[M + H]^+$ ion (Fig. S23 and S28‡). The complex **1** was also studied by UV–Vis absorption spectroscopy in dichloromethane solution recorded at room temperature. Ru(II) complex **1**, in dichloromethane, showed a strong absorption band with a maximum (λ_{abs}) around 320 nm and broad absorption bands with a maximum (λ_{abs}) around 383 nm. The higher energy absorption band is due to the effective π conjugation in the phosphole skeleton, whereas the lower energy band is assigned to metal to ligand charge transfer (MLCT) (Fig. S52‡).

The molecular structures of $[RuCl_2(\eta^6\text{-}p\text{-cymene})(L1\text{-}\kappa^1\text{-}P)]$ (1) and $[RuCl_2(\eta^6\text{-}p\text{-cymene})(L2\text{-}\kappa^1\text{-}P)]$ (2)

The perspective views of molecular structures **1** and **2** (data is of poor quality, given for reference only) along with the atom labelling are shown in Fig. 2. The crystallographic data and the details of the structure determination are given in the Experimental section (Table 1). The selected bond lengths (Å) and bond angles (°) are listed in Fig. 2. In complexes **1** and **2**, Ru^{II} adopts the pseudo-octahedral geometry with a *p*-cymene,

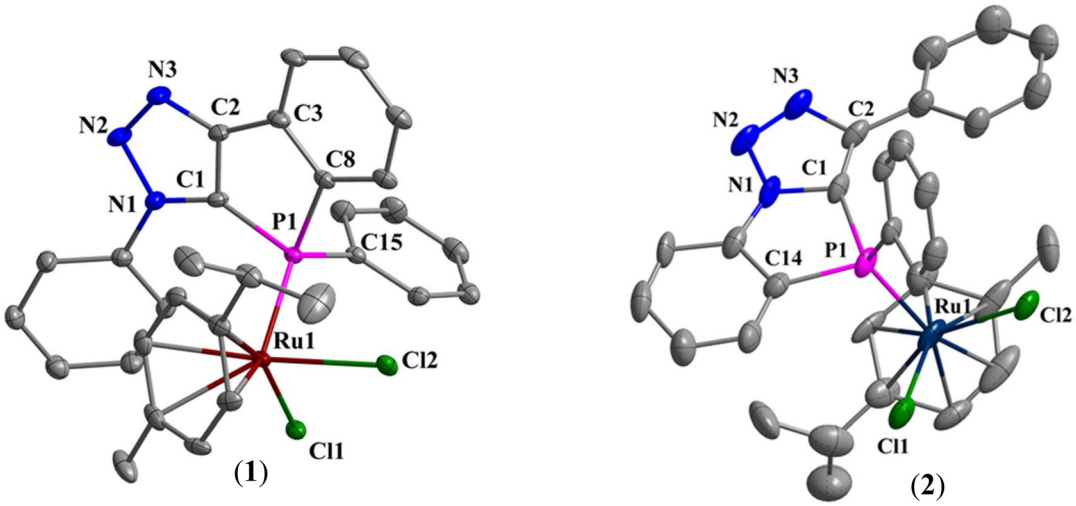

Fig. 2 The molecular $[RuCl_2(\eta^6\text{-}p\text{-cymene})(\mathbf{L1}\text{-}\kappa^1\text{-}P)]$ (**1**) and $[RuCl_2(\eta^6\text{-}p\text{-cymene})(\mathbf{L2}\text{-}\kappa^1\text{-}P)]$ (**2**). Hydrogen atoms have been omitted for clarity. Displacement ellipsoids are drawn at the 30% probability level. Selected bond lengths (Å) and bond angles (°): for complex **1**: C1–P1 1.813(3), C8–P1 1.851(3), C15–P1 1.824(3), P1–Ru1 2.3244(9), Ru1–Cl1 2.4021(9), Ru1–Cl2 2.4136(9), N1–C1 1.357(4), C2–C3 1.458(5), C3–C8 1.398(5) C1–P1–C8 88.39(16), C1–P1–C15 104.59(16), C1–P1–Ru1 115.02(12), C8–P1–Ru1 114.97(11), Cl1–Ru1–Cl2 = 86.36(3), P1–Ru1–Cl1 89.38(3), P1–Ru1–Cl2 86.20 (3). For complex **2**: C1–P1 1.837(8), C15–P1 C14–P1 1.873(9), P1–Ru1 2.348(2), Ru1–Cl1 2.409(3), Ru1–Cl2 2.402(2), N1–C1 1.392(9), C1–P1–C8 88.42(19), C1–P1–C14 89.2(4), C1–P1–Ru1 114.8(2), Cl1–Ru1–Cl1 = 88.24(8), P1–Ru1–Cl1 83.49(8), P1–Ru1–Cl2 89.46(7).

Table 1 Optimization of reaction conditions of benzylic C–H oxidation[a]

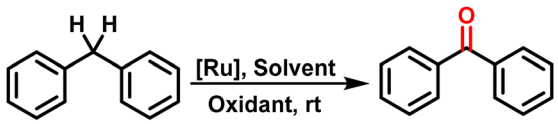

Entry	Cat. (mol %)	Oxidant (equiv)	Time (h)	Solvent	Conversion[b] [%]
1	—	TBHP (4)	1	CH_2Cl_2	NC[c]
2	**1** (0.2)	—	1	CH_2Cl_2	NC[c]
3	**2** (0.2)	TBHP (2)	1	CH_2Cl_2	61
4	**1** (0.2)	TBHP (2)	1	CH_2Cl_2	83
5	**1** (0.2)	H_2O_2 (3)	1	CH_2Cl_2	58
6	**1** (0.2)	CAN (3)	1	CH_2Cl_2	49
7	**1** (0.2)	*m*-CPBA (3)	1	CH_2Cl_2	39
8	**1** (0.2)	$NaIO_4$ (3)	1	CH_2Cl_2	14
9	**1** (0.2)	TBHP (3)	1	CH_2Cl_2	89
10	**1** (0.5)	TBHP (3)	1	CH_2Cl_2	94
11	**1 (0.5)**	**TBHP (4)**	**2**	**CH_2Cl_2**	**100**
12	**1** (0.5)	TBHP (4)	2	EtOH	48
13	**1** (0.5)	TBHP (4)	1	THF	35
14	**1** (0.5)	TBHP (4)	2	^{i}PrOH	54
15	**1** (0.5)	TBHP (4)	2	H_2O	17
16	$[Ru(p\text{-cymene})Cl_2]_2$ (0.5)	TBHP (4)	2	CH_2Cl_2	21
17	$RuCl_3{\cdot}3H_2O$ (0.5)	TBHP (4)	2	CH_2Cl_2	7

[a] Reaction conditions: diphenylmethane (0.5 mmol), Ru^{II} precatalyst (0.5 mol%), oxidant (4 equiv.), solvent (2 mL), rt, 2 h. [b] GC conversion. Abbreviations: [c] NC = no conversion, *p*-cym = *para*-cymene, TBHP = *tert*-butyl hydroperoxide.

two chloride and a phosphorus atom completing the coordination sphere. The Ru–P bond distances of 2.3244(9) and 2.348(2) Å in complexes **1** and **2** fall within a comparable range, so as Ru–Cl bond distances.[23] The P1–Ru1–Cl1 bond angle in complex **1** (89.38(3)°) is larger than that in **2** (83.49 (8)°), whereas the P1–Ru1–Cl2 and Cl1–Ru1–Cl2 bond angles in **1** (86.20(3)°) and **2** (88.24(8)°) lie within a fairly narrow deviation. The distance between the ruthenium center and centroid of *p*-cymene or proximal phenyl ring of ligand backbone is 1.70 Å and is independent of coordination geometry around the metal atoms. However, the average Ru–C(cymene) distance of 2.219 Å in **1** is in the range observed in complexes such as $[Ru(\eta^6\text{-}p\text{-cymene})Cl_2\{DippNHPPh_2\}\text{-}\kappa^1\text{-}P]$ (2.211(2) Å)[24] and $[RuCl_2(\eta^6\text{-}p\text{-cymene})\{(PPh_3)\text{-}\kappa^1\text{-}P\}]$ (2.218(2) Å).[25] The Ru–C bonds *trans* to the phosphorus atom (Ru(1)–C(26) = 2.243(4) and Ru(1)–C(25) = 2.239(3) Å) are slightly longer than those (2.160(3)–2.194(3) Å) *trans* to the two chloride ions. Similar trends were observed in related arene-ruthenium(II) complexes and attributed to the bond-lengthening effect of the phosphine ligands.[26] The (Ru–P 2.3246(10) Å) and (Ru–Cl 2.4022 (10) Å) bond distances are similar to those in $[Ru(\eta^6\text{-}p\text{-cymene})Cl_2(DippNHPPh_2)\text{-}\kappa^1\text{-}P]$ (2.372(5) and 2.418(6) Å),[26] $[\{Ru(\eta^6\text{-}p\text{-cymene})Cl_2\}_2\{(\mu\text{-DPEphos})\text{-}\kappa^1\text{-}P\}]$ (2.370(10) and 2.410(8) Å) and $[Ru(\eta^6\text{-}p\text{-cymene})Cl_2\{(PPh_3)\text{-}\kappa^1\text{-}P\}]$ (2.343(6) and 2.415(6) Å).[27]

Synthesis of Pd^{II} and Au^{I} complexes (3–6)

The reactions of **L1** and **L2** with $[Pd(COD)Cl_2]$ in 2 : 1 molar ratios afforded *trans*-$[PdCl_2(\mathbf{L1}\text{-}\kappa^1\text{-}P)_2]$ (**3**) and *trans*-$[PdCl_2(\mathbf{L2}\text{-}\kappa^1\text{-}P)_2]$ (**4**), respectively. Treatment of **L1** with $[Pd(\eta^3\text{-}C_3H_5)Cl]_2$ in 1 : 1 molar ratios in dichloromethane afforded square planar complexes $[Pd(\eta^3\text{-}C_3H_5)Cl(\mathbf{L1}\text{-}\kappa^1\text{-}P)]$ (**5**) as shown in Chart 2. The $^{31}P\{^1H\}$ NMR spectra of **3** and **4** showed two signals at −0.3 and −1.6 ppm and −1.3 and −2.6 ppm, respectively, probably due to the presence of SR/RS and RR/SS diastereomers (Fig S30 and S33‡). In both the complexes the ligands are in a mutually trans-disposition which is primarily due to

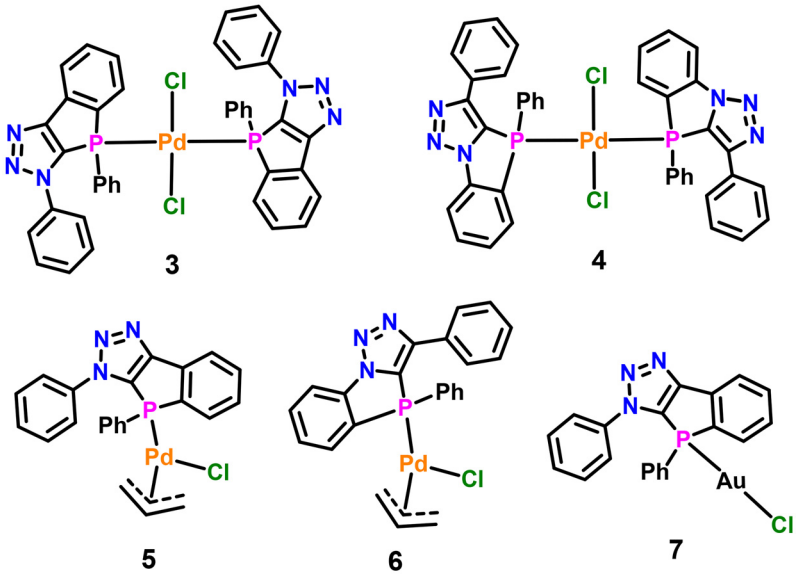

Chart 2 Pd^{II} and Au^{I} complexes **3–7**.

the steric bulk of the ligands.[27] Single-crystal X-ray analysis revealed the predominance of the SR|RS diastereomers in both **3** and **4**. The ^{31}P NMR spectrum of **5** showed a singlet at −3.0 ppm, whereas the ^{1}H NMR spectrum showed five allylic signals due to the asymmetry in the complex. The two upfield resonances around 3.0 and 2.3 ppm may be arising due to the CH_2 group *anti* to the chloride ion. The reaction of **L2** with $[Pd(\eta^3\text{-}C_3H_5)Cl]_2$ yielded a mixture of product evinced by ^{31}P NMR spectrum which showed two signals of nearly equal intensity, probably due the presence of $[Pd(\eta^3\text{-}C_3H_5)Cl(\mathbf{L2}\text{-}\kappa^1\text{-}P)]$ **6** (monomer) and its dimer having a $\{Pd(\mu\text{-}Cl)_2Pd\}$ moiety. While the mass spectrum predominantly displayed a peak corresponding to the monomer, it is noteworthy that, dimeric species often show mass signals consistent with the monomeric fragments.

Treatment of **L1** with $[AuCl(SMe_2)]$ in 1 : 1 molar ratio in dichloromethane afforded $[AuCl(\mathbf{L1}\text{-}\kappa^1\text{-}P)]$ (**7**) as a white solid. The $^{31}P\{^1H\}$ NMR spectrum of **7** showed a single resonance at 6.8 ppm (Fig. S45‡). In the ^{1}H NMR spectrum of **7** aromatic protons appeared in the range of 7.48–8.17 ppm. HRMS spectrum of **7** showed a molecular ion peak at 524.0581 corresponding to $[M - Cl]^+$ ions, and the molecular structure was confirmed by a single-crystal X-ray analysis.

Ru(II) catalyzed benzylic C–H oxidation reaction

Ru(II) complexes **1** and **2** were tested for their catalytic ability in the direct oxidation of aromatic hydrocarbons, such as benzylic C–H bonds, to the corresponding aromatic ketones (Table 1). Diphenylmethane was selected as a model substrate in the presence of *tert*-butyl hydroperoxide (TBHP) with CH_2Cl_2 as a solvent (Table 1). The oxidation of diphenylmethane was not observed in the absence of catalyst (**1**) and oxidant (TBHP) (Table 1, entries 1 and 2). Initially, complexes **1** and **2** were tested using 0.2 mol% of catalyst loading and TBHP (4 equiv.) as oxidant at room temperature in dichloromethane for 1 h. Complex **2** showed moderate activity and effected 61% conversion to form benzophenone (Table 1, entry 3), whereas complex **1** showed a relatively higher conversion (83%) (Table 1, entry 4). Oxidizing agents such as: H_2O_2, CAN, *m*-CPBA, and $NaIO_4$, produced low to moderate conversions (Table 1, entries 5–8), but TBHP worked well and hence used in subsequent reactions along with complex **1**.

The catalyst loading 0.2 mol% with 3 equiv. oxidant TBHP in 1 h showed up to 89% conversion (Table 1, entry 9). As a result, raising the catalyst loading from 0.2 to 0.5 mol% with 4 equiv. oxidant TBHP in 2 h resulted in 100% conversion (Table 1, entry 11). Later, the oxidation process was examined using Ru(II) complex **1**, and various solvents such as dichloromethane, ethanol, THF, ^{i}PrOH and H_2O, amongst dichloromethane was shown to be good solvent (Table 1, entries 12–15). Thus $RuCl_3{\cdot}3H_2O$ and $[Ru(p\text{-cymene})Cl_2]$ were poorly active in comparison with Ru(II) complex **1** (Table 1, entries 16 and 17). We found that the Ru(II) complex **1** (0.5 mol%) in the presence of TBHP (4 equiv.) in dichloromethane at room temperature showed the best conversion to form benzophenone in just 2 h. Also, ruthenium complex **1** with low catalyst loading and reduced time found to be much better than the similar ruthenium catalysts[28] used in benzylic C–H oxidation.

In order to demonstrate the breadth of the current methodology, many aromatic alkanes were examined using four equivalents of TBHP and 0.5 mol% of **1** at room temperature in dichloromethane (Chart 3). A series of benzylic hydrocarbons furnished the desired ketones in good to excellent yields (Chart 3, entries **1a–1i**). However, the ethyl groups at the *ortho* and *para* position of pyridines showed poor conversion (Chart 3, entries **1j–1k**). Phenylethanes containing either electron-neutral or electron-donating groups produced moderate yields of 44–56% (Chart 3, entries **1l–1o**).

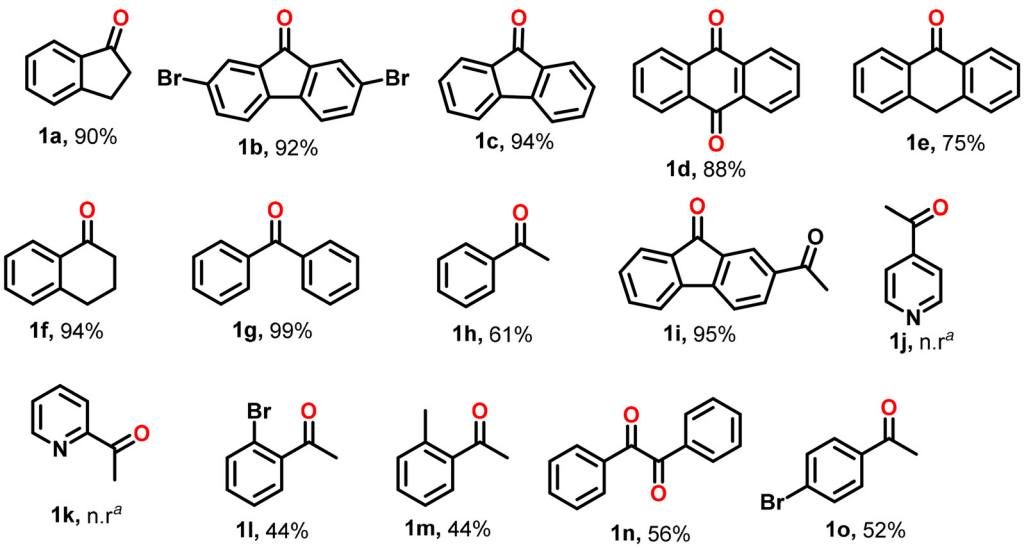

Chart 3 Substrates scope of benzylic C–H oxidation. Reaction conditions: substrate (0.5 mmol), Ru catalyst **1** (0.5 mol%), TBHP (**4** equiv.), CH_2Cl_2 (2 mL), rt, 2 h, all are isolated yields. [a] n.r. = no reaction.

Proposed mechanism for the benzylic C–H oxidation reaction

To elucidate the reaction mechanism, few controlled experiments were conducted. A radical quenching experiment was performed using 2,2,6,6-tetramethylpiperidine-1-oxyl (TEMPO) to gain insights into the oxidation process (Scheme 3a). The addition of 4 equiv. of TEMPO to the reaction mixture resulted in a significant reduction in the reaction rate. This observation suggests the involvement of a free radical pathway in the oxidation. It is hypothesized that, in the presence of ruthenium catalyst and TBHP, a carbon-centered radical is generated from the hydrocarbon substrate. This radical reacts with TEMPO to form a benzyl alcohol-TEMPO adduct, which was detected by low-resolution electrospray ionization mass spectrometry (ESI-MS) (Fig. S49‡). These findings support the proposed radical-based mechanism. Additionally, when diphenylmethanol was used, the corresponding ketone was formed in very low yield (Scheme 3b), indicating the fact that the benzylic alcohol does not act as an intermediate. However, when ethylbenzene was used as the substrate, the corresponding oxygenated product was detected after 75 minutes, suggesting its role as an intermediate in the reaction (Scheme 3c and Fig. S50‡).

Further, UV–Vis absorption spectra were taken to gain more insight into the nature of the intermediate(s), and to understand the probable pathway involved in this oxidative transformation. UV–Vis spectrum recorded for **1** at room temperature showed two absorption bands at 320 and 383 nm, which were shifted to 324 and 420 nm, upon addition of TBHP

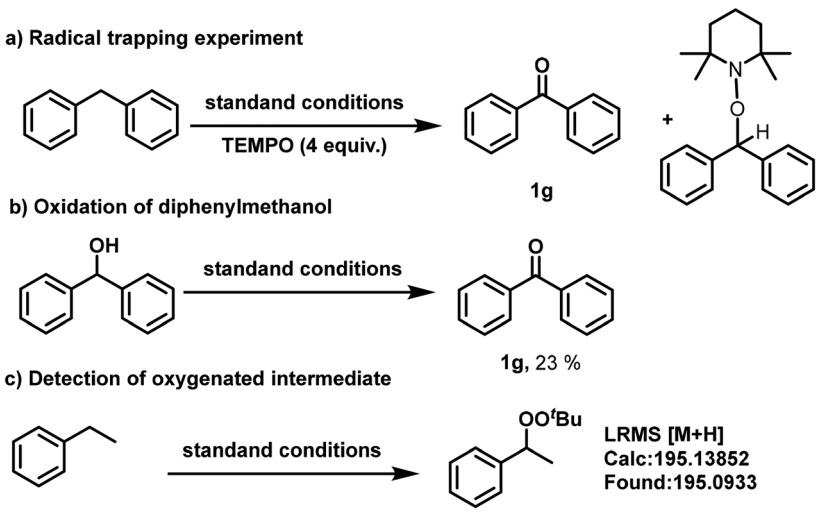

Scheme 3 (a–c) Controlled experiments.

(Fig. S52‡). The quenched characteristic MLCT band at 383 nm indicated the possible formation of a high-valent Ru-oxo species in the presence of TBHP. Similar spectral changes have been reported in the literature upon the addition of oxidants to Ru complexes, thus supporting the proposed formation of such intermediates in the reaction mechanism.[28b,29]

Based on the reported literature[28b] and experimental observations, a plausible mechanism for the Ru-catalyzed benzylic C–H oxidation is proposed (Scheme S1‡). Initially, TBHP reacts with complex **1** to form an intermediate **A**, which undergoes cleavage to generate a ^{t}BuO$^{\bullet}$ radical and Ru^{III}-OH species **B**, which was detected by LRMS (Fig. S51‡). The species **B** subsequently reacts with an additional equivalent of TBHP to form the Ru^{III}-OO^{t}Bu intermediate **C** along with water. Intermediate **C** then decomposes to release a ^{t}BuOO$^{\bullet}$ radical and regenerate **A**. The ^{t}BuO$^{\bullet}$ radical abstracts a hydrogen atom from the hydrocarbon substrate, forming a carbon-centered radical, which reacts with the ^{t}BuOO$^{\bullet}$ radical to produce an oxygenated intermediate. This intermediate undergoes further transformation to yield the corresponding ketone with the elimination of ^{t}BuOH.

Conclusions

In summary, new 1,2,3-triazole based phosphole and azaphosphole and their Ru(II), Pd(II) and Au(I) complexes were prepared and characterized using spectroscopic methods and single-crystal X-ray analysis. Ru(II) complex showed very good catalytic activity towards the oxidation of benzylic methylene with TBHP at room temperature. The phenylethane derivatives either with electron-neutral or electron-donating groups were oxidized to ketones with moderate to good conversions. Mechanistic studies by spectroscopic measurements including UV–Vis, ESI-MS, support the Ru(III) complex as an active intermediate involved in the oxidation reaction.

Experimental section

General procedures

All air-sensitive compounds were handled and stored in the MBRAUN Glovebox. All experimental manipulations were performed under dry nitrogen or argon using standard Schlenk techniques. All the solvents were purified by conventional procedures and distilled prior to use. $[Pd(COD)Cl_2]$,[30] $[Pd(\eta^3\text{-}C_3H_5)Cl]_2$[31] and $[AuCl(SMe_2)]$[32] were prepared according to the published procedures. Other reagents were obtained from commercial sources and used after purification.

Instrumentation

The ^{1}H and $^{31}P\{^{1}H\}$ NMR (δ in ppm) spectra were obtained on a BRUKER spectrometer operating at 400 and 500 MHz. The spectrum was recorded in $CDCl_3$ solutions with an internal lock; TMS and 85% H_3PO_4 were used as internal and external standards for ^{1}H and $^{31}P\{^{1}H\}$ NMR, respectively. Microanalyses were carried out on a Carlo Erba (model 1106) elemental analyzer. Melting points of all compounds were determined on a Veego melting point apparatus and are uncorrected.

Synthesis of $[C_6H_5\{1,2,3\text{-}N_3CC_6H_4C(PPh)\}]$ (L1) and $[C_6H_4\{1,2,3\text{-}N_3C(Ph)C(PPh)\}]$ (L2)

To a schlenk flask charged with 4-(2-bromophenyl)-1-phenyl-1*H*-1,2,3-triazole (0.50 g, 1.66 mmol) or 1-(2-bromophenyl)-4-phenyl-1*H*-1,2,3-triazole (0.50 g, 1.66 mmol) in Et_2O (30 mL) maintained at −78 °C, was added dropwise a solution of ^{n}BuLi (1.50 mL, 3.49 mmol, 1.6 M solution in hexane), room temperature and stirred for 6 h. Again, the solution was cooled to −78 °C and $PhPCl_2$ (0.297 g, 1.66 mmol) was added dropwise through a cannula. After the completion of the addition, the solution was slowly warmed to room temperature and stirred for 12 h. The LiCl salt was filtered off, the solvent was removed under reduced pressure and the residue obtained was purified by column chromatography on silica gel with ethyl acetate and petroleum ether as eluent to obtain **L1** and **L2**, respectively, as white crystalline solid. X-ray quality crystals of **L1** and **L2** were obtained by crystallizing in a 1 : 1 mixture of dichloromethane and petroleum ether at room temperature for 24 h. Yield: (0.30 g, 55% yield in case of **L1**; 0.250 g, 45% yield in case of **L2**). NMR data for compound **L1**: $^{31}P\{^{1}H\}$ NMR (162 MHz, $CDCl_3$): δ −39.5 (s). ^{1}H NMR (400 MHz, $CDCl_3$): δ 8.17 (d, J = 8.0 Hz, 1H), 7.88–7.84 (m, 2H), 7.66 (dd, J = 7.4, 4.8 Hz, 1H), 7.62–7.58 (m, 1H), 7.42–7.37 (m, 5H), 7.35–7.29 (m, 4H). $^{13}C\{^{1}H\}$ NMR (101 MHz, $CDCl_3$): δ 148.6, 138.0, 135.2 (d, J = 12.0 Hz), 133.5, 133.3, 131.8, 131.6, 131.0, 130.6, 129.5, 129.4, 129.0, 128.5, 128.1 (d, J = 7.2 Hz), 126.3 (d, J = 3.2 Hz). FT-IR (KBr disk, cm^{-1}): 3062 s, 1603 w, 1459 w, 1206 s, 1557 w, 994 s, 769 m, 692 w. HRMS calc. for $C_{20}H_{14}N_3P_1$ $[M + H]^+$ 328.0998, found 328.0997. Anal. calcd for $C_{20}H_{14}N_3P$: C, 73.39; H, 4.31; N, 12.84. found: C, 73.48; H, 4.28; N, 12.80. NMR data for compound **L2**: $^{31}P\{^{1}H\}$ NMR (162 MHz, $CDCl_3$): δ −32.9 (s). ^{1}H NMR (400 MHz, $CDCl_3$): δ 8.13 (dd, J = 7.6, 1.0 Hz, 1H), 7.73–7.69 (m, 2H), 7.59–7.51 (m, 2H), 7.46–7.42 (m, 2H), 7.40–7.35 (m, 4H), 7.33–7.27 (m, 3H). $^{13}C\{^{1}H\}$ NMR (101 MHz, $CDCl_3$): δ 145.5, 137.6, 134.1, 133.8, 131.2, 131.1, 130.9, 129.8, 129.6, 129.4, 129.3, 128.7, 127.9 (d, J = 8.9 Hz), 121.9, 120.5 (d, J = 3.8 Hz). FT-IR (KBr disk, cm^{-1}): 3022 s, 1503 w, 1420 w, 1200 s, 1457 w, 984 s, 779 m, 622 w. HRMS calc. for $C_{20}H_{14}N_3P_1$ $[M + H]^+$ 328.0998, found 328.0991. Anal. calcd for $C_{20}H_{14}N_3P$: C, 73.39; H, 4.31; N, 12.84. Found: C, 73.46; H, 4.27; N, 12.82.

Synthesis of $[C_6H_5\{1,2,3\text{-}N_3CC_6H_4C(P(O)Ph)\}]$ ($L1_O$)

H_2O_2 (0.025 mL, 0.150 mmol, 30% H_2O_2) was added to a solution of **L1** (0.045 g, 0.137 mmol) in THF (30 mL). The reaction mixture was stirred at room temperature for 12 h. After removing the solvents under reduced pressure, the white sticky oil obtained was washed with petroleum ether (3 × 10 mL) to give analytically pure compound $\mathbf{L1_O}$ as a white solid. Yield: (0.023 g, 56%). Mp 220–222 °C. $^{31}P\{^{1}H\}$ NMR (162 MHz, $CDCl_3$): δ 11.5 (s). ^{1}H NMR (400 MHz, $CDCl_3$): δ 8.17–8.12 (m, 1H), 8.04–7.97 (m, 2H), 7.85–7.79 (m, 2H), 7.76–7.70 (m, 2H), 7.59–7.52 (m, 2H), 7.48–7.40 (m, 5H). FT-IR (KBr disk, cm^{-1}):

2964 s, 2930 s, 2023 w, 1415 s, 1262 s, 1203 s, 1119 s, 1037 s, 763 s, 553 s. HRMS calc. for $C_{20}H_{14}N_6P_2O_2$ $[M + H]^+$ 344.0947, found 344.0941. Anal. calcd for $C_{20}H_{14}N_3PO$: C, 69.97; H, 4.11; N, 12.24. Found: C, 69.90; H, 4.19; N, 12.10.

Synthesis of [C_6H_4{1,2,3-$N_3C(Ph)C(P(O)Ph)$}] ($L2_O$)

A procedure similar to that of $L1_O$ was used by taking H_2O_2 (0.02 mL, 0.150 mmol, 30% H_2O_2) and **L2** (0.045 g, 0.137 mmol) to obtain an analytically pure product of $L2_O$ as white solid. Yield: (0.025 g, 61%). Mp: 225–227 °C(dec.). $^{31}P\{^1H\}$ NMR (162 MHz, $CDCl_3$): δ 14.1 (s).

^1H NMR (400 MHz, $CDCl_3$) δ 8.01–7.96 (m, 2H), 7.96–7.94 (m, 1H), 7.73–7.65 (m, 4H), 7.55–7.49 (m, 3H), 7.47–7.39 (m, 4H). FT-IR (KBr disk, cm^{-1}): 2854 s, 2820 s, 2022 w, 1386 s, 1152 s, 1103 s, 1159 s, 1127 s, 757 s, 525 s. HRMS calc. for $C_{20}H_{14}N_6P_2O_2$ $[M + H]^+$ 344.0947, found 344.0941. Anal. calcd for $C_{20}H_{14}N_3PO$: C, 69.97; H, 4.11; N, 12.24. Found: C, 69.76; H, 4.23; N, 12.31.

Synthesis of [$RuCl_2$(η^6-*p*-cymene){C_6H_5(1,2,3-$N_3CC_6H_4C(PPh)$)-κ^1-*P*}] (1)

A solution of $[Ru(\text{-}p\text{-cymene})Cl_2]_2$ (0.028 g, 0.0458 mmol) in dichloromethane (3 mL) was added dropwise to a solution of **L1** (0.030 g, 0.091 mmol) also in dichloromethane (4 mL) and stirred for 4 h at room temperature. The solvent was removed under reduced pressure and the residue obtained was washed with petroleum ether (2 × 10 mL) and dried under vacuum to give compound **1** as a red solid. The crystals of **1** suitable for single-crystal X-ray diffraction study were obtained by crystallizing in a 1 : 1 mixture of chloroform and petroleum ether at room temperature over 30 h. Yield: 80% (0.029 g). Mp: 215–217 °C, $^{31}P\{^1H\}$ NMR (162 MHz, $CDCl_3$): δ −0.1 (s). ^1H NMR (400 MHz, $CDCl_3$): δ 8.29 (t, J = 8.2 Hz, 1H), 8.11 (d, J = 7.6 Hz, 1H), 8.01 (d, J = 8.0 Hz, 2H), 7.91–7.83 (m, 2H), 7.59 (t, J = 7.5 Hz, 1H), 7.53–7.48 (m, 2H), 7.43–7.34 (m, 3H), 7.24 (dd, J = 7.5, 3.1 Hz, 2H), 5.11 (d, J = 6.1 Hz, 1H), 5.04 (d, J = 6.2 Hz, 1H), 4.89 (d, J = 6.0 Hz, 1H), 4.63 (d, J = 5.9 Hz, 1H), 2.26 (q, J = 7.1 Hz, 1H), 1.51 (s, 3H), 0.91 (d, J = 6.9 Hz, 3H), 0.83 (d, J = 6.9 Hz, 3H). FT-IR (KBr disk, cm^{-1}): 3241 w, 2967 s, 1731 s, 1626 w, 1566 s, 1414 s, 1262 s, 1092 s, 1023 w, 847 w, 77 w, 547 s. HRMS calc. for $C_{30}H_{28}ClN_3PRu$ $[M - Cl]^+$ 598.0747, found 598.0755. Anal. calcd for $C_{30}H_{28}N_3PRuCl_2$: C, 56.88; H, 4.45; N, 6.63. Found: C, 56.75; H, 4.46; N, 6.60.

Synthesis of [$RuCl_2$(η^6-*p*-cymene){C_6H_4(1,2,3-$N_3C(Ph)C(PPh)$)-κ^1-*P*}] (2)

A procedure similar to that of **1** was used by taking solution of $[Ru(\text{-}p\text{-cymene})Cl_2]_2$ (0.028 g, 0.0458 mmol) in dichloromethane (3 mL) was added dropwise to a solution of **L2** (0.033 g, 0.057 mmol) in dichloromethane (4 mL) and stirring for 4 h at room temperature. The solvent was removed under reduced pressure and the residue obtained was washed with petroleum ether (3 × 5 mL) and dried under vacuum to give compound **2** as a red solid. X-ray quality crystals of **2** were obtained by crystallizing in a 1 : 1 mixture of dichloromethane and petroleum ether at room temperature for 10 h. Yield: 72% (0.026 g) Mp: 170–175 °C, $^{31}P\{^1H\}$ NMR (162 MHz, $CDCl_3$): δ −3.9 (s). ^1H NMR (400 MHz, $CDCl_3$): δ 8.55 (t, J = 7.6 Hz, 1H), 8.19–8.16 (m, 2H), 7.84 (dd, J = 12.1, 7.8 Hz, 2H), 7.69 (t, J = 7.7 Hz, 1H), 7.57–7.41 (m, 4H), 7.38 (dd, J = 8.4, 6.3 Hz, 1H), 5.27 (d, J = 6.2 Hz, 1H), 5.16 (d, J = 6.2 Hz, 1H), 4.99–4.88 (m, 1H), 4.69 (d, J = 5.8 Hz, 1H), 2.39–2.31 (m, 1H), 1.37–1.18 (m, 3H), 0.97 (d, J = 7.0 Hz, 3H), 0.85 (d, J = 6.8 Hz, 3H). ^{13}C NMR (101 MHz, $CDCl_3$): δ 134.0, 133.9, 133.3, 133.2, 132.4, 131.5, 129.7, 129.4, 129.0, 128.9, 128.7, 128.6, 128.4, 127.8, 113.9, 109.4, 101.3, 90.2, 90.1, 89.8, 86.3, 85.0, 30.2, 22.0, 21.3, 17.7. FT-IR (KBr disk, cm^{-1}): 3059 w, 2967 s, 1644 s, 1558 m, 1416 s, 1103 w, 1023 s, 847 s, 774 s, 694 w, 547 m. HRMS calc. for $C_{30}H_{28}Cl_1N_3P_1Ru_1$ $[M - Cl]^+$ 598.0747, found 598.0755. Anal. calcd for $C_{30}H_{28}N_3PRuCl_2$: C, 56.88; H, 4.45; N, 6.63 found: C, 56.62; H, 4.65; N, 6.41.

Synthesis of *trans*-[$PdCl_2$(L1-κ^1-*P*)$_2$] (3)

To a stirred solution of $[Pd(COD)Cl_2]$ (0.013 g, 0.045 mmol) in dichloromethane (4 mL) was added dropwise a solution of **L1** (0.03 g, 0.091 mmol) also in dichloromethane (4 mL) and the reaction mixture was stirred for 4 h at room temperature. The solvent was removed under reduced pressure and the residue obtained was washed with petroleum ether (2 × 8 mL) and dried under vacuum to give compound **3** as a yellow solid. The crystals of **3** suitable for X-ray analysis were obtained by crystallizing in a 1 : 1 mixture of dichloromethane and petroleum ether stored at room temperature for 20 h. Yield: 79% (0.060 g). Mp: 180–183 °C. $^{31}P\{^1H\}$ NMR (162 MHz, $CDCl_3$): δ −0.3 (s, SS/RR, 21%), −1.6 (s, SR\RS, 79%). ^1H NMR (400 MHz, $CDCl_3$): δ 9.94 (d, J = 5.9 Hz, 2H), 8.62 (d, J = 7.9 Hz, 2H), 8.06 (d, J = 9.6 Hz, 2H), 7.50 (dd, J = 15.1, 7.5 Hz, 14H), 7.07 (d, J = 7.3 Hz, 4H), 6.82 (d, J = 8.3 Hz, 4H). HRMS calc. for $C_{40}H_{48}Cl_2N_6P_2Pd$ $[M + H]^+$ 851.1900, found 853.1881.

Synthesis of *trans*-[$PdCl_2$(L2-κ^1-*P*)$_2$] (4)

A procedure similar to **3** was used by taking a stirred solution of $[Pd(COD)Cl_2]$ (0.013 g, 0.045 mmol) in dichloromethane (4 mL) was added dropwise a solution of **L2** (0.030 g, 0.091 mmol) in the same solvent dichloromethane (4 mL) and stirring for 4 h at room temperature. The solvent was removed under reduced pressure and the residue obtained was washed with petroleum ether (2 × 10 mL) and dried under vacuum to give compound **4** as a yellow solid. Yield: 65% (0.030 g). Mp: 190–193 °C. $^{31}P\{^1H\}$ NMR (162 MHz, $CDCl_3$): δ −1.3 (s, RS/RS, 60%), −2.6 (s, SS/RR, 40%). ^1H NMR (500 MHz, $CDCl_3$) δ 7.99–7.90 (m, 1H), 7.65 (t, J = 6.5 Hz, 1H), 7.38–7.11 (m, 11H), 6.95 (t, J = 7.6 Hz, 1H). ^1H NMR (500 MHz, $CDCl_3$) δ 8.16–8.19 (m, 1H), 7.80–7.74 (m, 2H), 7.53 (h, J = 7.7 Hz, 9H), 7.07 (t, J = 7.3 Hz, 2H). FT-IR (KBr disk, cm^{-1}): 3359 w, 1636 s, 1568 s, 1415 s, 1098 s, 548 w. HRMS calc. for $C_{23}H_{19}N_3PPd$ $[M - Cl]^+$ 474.0346, found 474.0354.

Synthesis of [Pd(η^3-C_3H_5)Cl(L1-κ^1-*P*)] (5)

To a stirred solution of $[Pd(\eta^3\text{-}C_3H_5)Cl]_2$ (0.016 g, 0.045 mmol) in dichloromethane (4 mL) was added dropwise a solution of **L1** (0.03 g, 0.091 mmol) also in dichloromethane (4 mL) and

the reaction mixture was stirred for 4 h at room temperature. The solvent was removed under reduced pressure and the residue obtained was washed with petroleum ether (3 × 6 mL) and dried under vacuum to give compound **5** as a red solid. Single-crystal suitable for X-ray diffraction was grown from a (1 : 1) mixture of CH_2Cl_2 and petroleum ether. Yield 72% (0.033 g) Mp: 210–214 °C. $^{31}P\{^1H\}$ NMR (162 MHz, $CDCl_3$): δ −3.0 (s). ^1H NMR (400 MHz, $CDCl_3$): δ 8.17–8.06 (m, 2H), 7.81 (s, 2H), 7.62–7.56 (m, 3H), 7.46–7.32 (m, 7H), 5.31 (s, 1H), 4.78 (s, 1H), 3.70 (s, 1H), 3.00 (s, 1H), 2.41–2.22 (m, 1H). HRMS calc. for $C_{23}H_{19}N_3P_1Pd_1$ $[M - Cl]^+$ 474.0346, found 474.0354. Anal. calcd for $C_{23}H_{19}N_3PPdCl$: C, 54.14; H, 3.75; N, 8.24. Found: C, 54.02; H, 3.62; N, 8.14.

Synthesis of [Pd(η³-C₃H₅)Cl(L2-κ¹-*P*)] (6)

A procedure similar to **5** was used by taking a stirred solution of $[Pd(\eta^3\text{-}C_3H_5)Cl]_2$ (0.016 g, 0.045 mmol) in dichloromethane (4 mL) was added dropwise a solution of **L2** (0.030 g, 0.091 mmol) in dichloromethane (5 mL) and stirring for 4 h at room temperature. The solvent was removed under reduced pressure and the residue obtained was washed with petroleum ether (2 × 10 mL) and dried under vacuum to give compound **6** as a yellow solid. Yield: 68% (0.031 g). Mp: 225–227 °C. $^{31}P\{^1H\}$ NMR (162 MHz, $CDCl_3$): δ −7.9 (s, 53%), −8.7 (s, 47%). ^1H NMR (400 MHz, $CDCl_3$) δ 8.16 (s, 2H), 7.52–7.38 (m, 12H), 4.80 (s, 1H), 3.34 (s, 1H), 3.21–2.90 (m, 2H), 2.41 (d, J = 10.2 Hz, 1H). HRMS calc. for $C_{23}H_{19}N_3P_1Pd_1$ $[M - Cl]^+$ 474.0346, found 474.0354.

Synthesis of [AuCl(L1-κ¹-*P*)] (7)

A solution of $AuCl(SMe_2)$ (0.029 g, 0.097 mmol) in dichloromethane (8 mL) was added dropwise to a solution of **L1** (0.032 g, 0.097 mmol) in the same solvent (8 mL) and the solution was stirred at room temperature for 5 h. After the complete removal of solvent under reduced pressure, the residue obtained was washed with petroleum ether (1 × 8 mL) and dried under vacuum to give **7** as a colorless solid. The crystals of **7** suitable for single-crystal X-ray diffraction study were obtained by crystallizing in 1 : 1 mixture of chloroform and petroleum ether at room temperature over 36 h. Yield: 90% (0.066 g). Mp: 210–214 °C (dec.). $^{31}P\{^1H\}$ NMR (162 MHz, $CDCl_3$) δ 6.8 (s). ^1H NMR (400 MHz, $CDCl_3$) δ 8.18–8.14 (m, 1H), 7.73–7.70 (m, 3H), 7.68–7.61 (m, 3H), 7.57–7.37 (m, 7H). FT-IR (KBr disk, cm^{-1}): 3055 s, 1650 s, 1565 w, 1385 s, 1102 s, 1040 s, 764 s, 567 s. HRMS calc. for $C_{20}H_{14}Au1N_3P_1$ $[M - Cl]^+$ 524.0586, found 853.1881. Anal. calcd for $C_{20}H_{14}Au_1Cl_1N_3P_1$: C, 42.92; H, 2.52; N, 7.51. Found: C, 43.25; H, 2.24; N, 7.27.

General procedure for Ru(II) catalysed C–H oxidation

Hydrocarbons (1 equiv.), Ru catalyst (0.5 mol%), and TBHP (4.0 mmol) were added to 2 mL of CH_2Cl_2 in a 5 mL reaction tube. The solution was stirred at room temperature for 2 h under open atmosphere. The residual mixture was diluted with H_2O (10 mL) and extracted twice with ethyl acetate (10 mL). The combined organic fractions were dried over Na_2SO_4, and the solvent was evaporated under reduced pressure to give crude product. The crude products were purified by silica gel column chromatography using petroleum ether/ethyl acetate as eluent.

Crystal structure determination of compounds L1, L2, 1–4, and 7

Single crystals of all compounds were mounted on a Cryoloop with a drop of Paratone oil and positioned in the cold nitrogen stream on a Rigaku Saturn724+ (2 × 2 bin mode) diffractometer. The data collections were performed at 150 K using a graphite monochromated Mo-Kα (λ = 0.71073) radiation source for **L1**, **L2**, **1–3**, **5** and **7** with the ω-scan technique [data for **2**, **3**, **5** and **7** are not publishable. Several attempts to obtaine X-ray good quality single crystals have been unsuccessful. As a result, the data is not deposited with CCDC, but structural description is given in ESI‡]. The data were reduced using CrysalisPro Red 171.41_64.93a software. The structures were solved using Olex2[33] with the ShelXT[34] structure solution program using intrinsic phasing and refined with the ShelXL[35] refinement package using least-squares minimization. All non-hydrogen atoms were refined anisotropically. Hydrogen atoms were placed in calculated positions and included as riding contributions with isotropic displacement parameters tied to those of the attached non-hydrogen atoms. In the given chemical formula and other crystal data, the unknown solvent molecule(s) are not considered. The reflections with error/esd more than 10 were excluded in order to avoid problems related to better refinement of the data. The data completeness is more than 99.8% in most of the cases, which is enough to guarantee a very good refinement of data. The details of X-ray structural determinations are given in Tables S1 and S2.‡ Crystallographic data for the structures reported in this paper have been deposited with the Cambridge Crystallographic Data Centre. CCDC 2403173 (compound **L1**), 1832215 (compound **L2**), and 2403174 (compound **2**)‡ contain the supplementary crystallographic data for this paper.

Data availability

The data supporting this article have been included as part of the ESI.‡

Crystal structure determination of compounds (CIFs).
NMR, HRMS and FT-IR spectra of compounds **1–7**.
NMR and Mass spectra of catalytic products.

Conflicts of interest

The authors declare no conflict of interest.

Acknowledgements

MSB thanks IIT Bombay for supporting this work through Research Development Fund (RDF). We also thank the

Department of Chemistry, Indian Institute of Technology Bombay, Mumbai, for instrumentation facilities.

References

1 M. Stolar and T. Baumgartner, *Chem. – Asian J.*, 2014, **9**, 1212–1225.
2 K. Fourmy, D. H. Nguyen, O. Dechy-Cabaret and M. Gouygou, *Catal. Sci. Technol.*, 2015, **5**, 4289–4323.
3 (*a*) R. A. Adler, C. Wang, A. Fukazawa and S. Yamaguchi, *Inorg. Chem.*, 2017, **56**, 8718–8725; (*b*) M. P. Duffy, W. Delaunay, P. A. Bouit and M. Hissler, *Chem. Soc. Rev.*, 2016, **45**, 5296–5310.
4 (*a*) G. S. Ananthnag and M. S. Balakrishna, in *Comprehensive Heterocyclic Chemistry IV*, Elsevier, Oxford, 2022, pp. 735–767; (*b*) G. S. Ananthnag and M. S. Balakrishna, in *Comprehensive Heterocyclic Chemistry IV*, Elsevier, Oxford, 2022, pp. 711–748.
5 D. Miesel, A. Hildebrandt, M. Korb, P. J. Low and H. Lang, *Organometallics*, 2013, **32**, 2993–3002.
6 Y. Ren and T. Baumgartner, *J. Am. Chem. Soc.*, 2011, **133**, 1328–1340.
7 (*a*) K. Baba, M. Tobisu and N. Chatani, *Angew. Chem., Int. Ed.*, 2013, **52**, 11892–11895; (*b*) Y. Unoh, K. Hirano, T. Satoh and M. Miura, *Angew. Chem., Int. Ed.*, 2013, **52**, 12975–12979.
8 Y. Matano, M. Nakashima, A. Saito and H. Imahori, *Org. Lett.*, 2009, **11**, 3338–3341.
9 X. He, P. Zhang, J.-B. Lin, H. V. Huynh, S. E. Navarro Muñoz, C.-C. Ling and T. Baumgartner, *Org. Lett.*, 2013, **15**, 5322–5325.
10 (*a*) S. Sheokand, S. Sharma, M. A. Mohite, G. Rajaraman and M. S. Balakrishna, *Chem. Commun.*, 2024, **60**, 7733–7736; (*b*) L. Radhakrishna, S. Sheokand, D. Mondal and M. S. Balakrishna, *Inorg. Chem.*, 2024, **63**, 9919–9930; (*c*) P. K. Namdeo, S. Sheokand, B. S. Kote, L. Radhakrishna, H. S. Kunchur, P. Saini, S. Ramakrishnan and M. S. Balakrishna, *Dalton Trans.*, 2022, 6795–6808; (*d*) B. Kaur, R. Gourkhede and M. S. Balakrishna, *Inorg. Chem.*, 2024, **63**, 16981–16990; (*e*) B. S. Kote, H. S. Kunchur, L. Radhakrishna, M. K. Pandey and M. S. Balakrishna, *Dalton Trans.*, 2021, **50**, 16782–16794.
11 D. G. Holah, A. N. Hughes and B. C. Hui, *Can. J. Chem.*, 1972, **50**, 3714–3718.
12 D. Neibecker, R. Reau and S. Lecolier, *J. Org. Chem.*, 1989, **54**, 5208–5210.
13 N. Mézailles, L. Ricard and F. Gagosz, *Org. Lett.*, 2005, **7**, 4133–4136.
14 (*a*) Y. Qiu and S. Gao, *Nat. Prod. Rep.*, 2016, **33**, 562–581; (*b*) W. R. Gutekunst and P. S. Baran, *Chem. Soc. Rev.*, 2011, **40**, 1976–1991; (*c*) J. F. Van Humbeck, *Synlett*, 2018, 1669–1674.
15 (*a*) A. J. Pearson and G. R. Han, *J. Org. Chem.*, 1985, **50**, 2791–2792; (*b*) B. M. Choudary, A. D. Prasad, V. Bhuma and V. Swapna, *J. Org. Chem.*, 1992, **57**, 5841–5844.
16 G. Blay, I. Fernández, T. Giménez, J. R. Pedro, R. Ruiz, E. Pardo, F. Lloret and M. C. Muñoz, *Chem. Commun.*, 2001, 2102–2103.
17 S. Murahashi, T. Naota and K. Yonemura, *J. Am. Chem. Soc.*, 1988, **110**, 8256–8258.
18 (*a*) C. S. Yi, K.-H. Kwon and D. W. Lee, *Org. Lett.*, 2009, **11**, 1567–1569; (*b*) S.-I. Murahashi, Y. Oda, T. Naota and T. Kuwabara, *Tetrahedron Lett.*, 1993, **34**, 1299–1302.
19 (*a*) P. Li and H. Alper, *J. Mol. Struct.*, 1990, **61**, 51–54; (*b*) M. Jurado-Gonzalez, A. C. Sullivan and J. R. H. Wilson, *Tetrahedron Lett.*, 2003, **44**, 4283–4286; (*c*) E. Modica, G. Bombieri, D. Colombo, N. Marchini, F. Ronchetti, A. Scala and L. Toma, *Eur. J. Org. Chem.*, 2003, 2964–2971.
20 (*a*) A. J. Catino, J. M. Nichols, H. Choi, S. Gottipamula and M. P. Doyle, *Org. Lett.*, 2005, **7**, 5167–5170; (*b*) A. Wusiman, X. Tusun and C.-D. Lu, *Eur. J. Org. Chem.*, 2012, 3088–3092.
21 L.-Q. Yang, K.-B. Wang and C.-Y. Li, *Eur. J. Org. Chem.*, 2013, 2775–2779.
22 (*a*) L. Radhakrishna, B. S. Kote, H. S. Kunchur, M. K. Pandey, D. Mondal and M. S. Balakrishna, *Dalton Trans.*, 2022, **51**, 5480–5493; (*b*) L. Radhakrishna, H. S. Kunchur, P. K. Namdeo, R. J. Butcher and M. S. Balakrishna, *Dalton Trans.*, 2020, **49**, 3434–3449.
23 (*a*) J. W. Faller and D. G. D'Alliessi, *Organometallics*, 2003, **22**, 2749–2757; (*b*) D. Arquier, L. Vendier, K. Miqueu, J.-M. Sotiropoulos, S. Bastin and A. Igau, *Organometallics*, 2009, **28**, 4945–4957.
24 M. Novák, M. Bouška, L. Dostál, M. Lutter, K. Jurkschat, J. Turek, F. De Proft, Z. Růžičková and R. Jambor, *Eur. J. Inorg. Chem.*, 2017, **2017**, 1292–1300.
25 M. R. J. Elsegood, M. B. Smith and N. M. Sanchez-Ballester, *Acta Crystallogr., Sect. E:Struct. Rep. Online*, 2006, **62**, m2838–m2840.
26 (*a*) S. Doherty, J. G. Knight, C. R. Addyman, C. H. Smyth, N. A. B. Ward and R. W. Harrington, *Organometallics*, 2011, **30**, 6010–6016; (*b*) R. Venkateswaran, J. T. Mague and M. S. Balakrishna, *Inorg. Chem.*, 2007, **46**, 809–817.
27 Z. Kokan, B. Perić, G. Kovačević, A. Brozovic, N. Metzler-Nolte and S. I. Kirin, *Eur. J. Inorg. Chem.*, 2017, **2017**, 3928–3937.
28 (*a*) S.-F. Hsu and B. Plietker, *ChemCatChem*, 2013, **5**, 126–129; (*b*) S. Kong, R. Liu, Z. Hao, Z. Han, G.-L. Lu and J. Lin, *J. Mol. Struct.*, 2024, **1296**, 136870; (*c*) S. K. Gupta and J. Choudhury, *ChemCatChem*, 2017, **9**, 1979–1984.
29 C.-B. Bo, Q. Bu, X. Li, G. Ma, D. Wei, C. Guo, B. Dai and N. Liu, *J. Org. Chem.*, 2020, **85**, 4324–4334.
30 D. Drew, J. R. Doyle and A. G. Shaver, *Inorg. Synth.*, 1990, **28**, 346–349.
31 Y. Tatsuno, T. Yoshida, S. Otsuka, N. Al-Salem and B. L. Shaw, *Inorg. Synth.*, 1990, **28**, 342–345.
32 M.-C. Brandys, M. C. Jennings and R. J. Puddephatt, *J. Chem. Soc., Dalton Trans.*, 2000, 4601–4606.
33 O. V. Dolomanov, L. J. Bourhis, R. J. Gildea, J. A. K. Howard and H. Puschmann, *J. Appl. Crystallogr.*, 2009, **42**, 339–341.
34 G. M. Sheldrick, *Acta Crystallogr.*, 2015, **71**, 3–8.
35 G. W. Sheldrick, *Acta Crystallogr.*, 2008, **A64**, 112–122.

